Scripta Materialia 145 (2018) 85–89

Contents lists available at ScienceDirect

Scripta Materialia

journal homepage: www.elsevier.com/locate/scriptamat

Regular article

Partial dislocation in carbon-vacancy-ordered $Nb_{12}Al_3C_8$

Hui Zhang [a], Xiaohui Wang [a,*], Erdong Wu [a], Yanchun Zhou [b,*]

[a] Shenyang National Laboratory for Materials Science, Institute of Metal Research, Chinese Academy of Sciences, 72 Wenhua Road, Shenyang 110016, China
[b] Science and Technology on Advanced Functional Composite Laboratory, Aerospace Research Institute of Materials & Processing Technology, Beijing 100076, China

ARTICLE INFO

Article history:
Received 3 September 2017
Accepted 14 October 2017
Available online xxxx

Keywords:
Dislocation
Stacking fault
MAX phase
Layered structure

ABSTRACT

Basal dislocations in nanolaminated machinable ternary carbides and nitrides (also known as MAX phases) have been postulated to be the result of shearing M—A bonds, but have not been microscopically confirmed yet. This study on dislocations and stacking faults in C-vacancy-ordered $Nb_{12}Al_3C_8$ demonstrates that the basal dislocation core lies between NbC slabs, verifying the shear of Nb—Al bonds. The formation of observed $1/3\langle 01\bar{1}0\rangle$ type partial dislocations therefore does not give rise to stacking faults. The frequently observed stacking faults are special intergrowth structures of atomically thin NbC slabs embedded in the $Nb_{12}Al_3C_8$ grain.

As atomically thin metal-ceramic multilayer laminates, MAX (M is an early transition metal element; A is an A group element; and X is C and/or N) phases possess the merits of ceramics and metals and have attracted ever-increasing interests [1–6]. Serving as the main carrier of plasticity, dislocations play a key role in the strength and ductility. Knowledge about the material-specific dislocation behavior is crucial not only to understand the mechanical response of materials but also to develop advanced structural materials [7,8]. Due to remarkably high c/a (3.5 ~ 7.8), basal dislocations in MAX phases are more likely confined within the basal plane than those in common hexagonal-close-packed (HCP) metals ($c/a < 2$) [7,9–15]. It is well-accepted that the dislocations in the as-sintered MAX phases and those uniaxially-deformed are basal type belonging to either basal or non-basal slip systems, although nonbasal dislocations have been observed under complex loading conditions [16–18]. These dislocations are prone to forming dislocation walls [11] and dislocation networks [19] or piling up at grain boundaries [20]. Recently, the dislocation core structure of MAX phases has been investigated using density functional theory and the Peierls–Nabarro–Galerkin model [21]. It is reported that $1/3\langle 11\bar{2}0\rangle$ type full dislocation could decompose into two mixed $1/3\langle 01\bar{1}0\rangle$ type partial dislocations. Specifically, the screw, 30°, 60° and edge full dislocations dissociate into two 30°, a screw and 60°, an edge and 30°, and two 60° partial dislocations, respectively. The separating distance between partial dislocations is found to be smaller than 7 Å. Theoretically, the partial dislocations and formed stacking faults cannot be observed by conventional diffraction contrast method (the spatial resolution of weak beam dark field is on the order of several nanometers [22]). Therefore, the existence of partial dislocations in MAX phases remains debatable. However, stacking faults extending a few micrometers have been ubiquitously observed in MAX phases [15,23,24]. Yu et al. pointed out that the stacking faults in Ti_3SiC_2 is caused by the insertion or extraction of TiC slabs into or from Ti_3SiC_2 resembling the intrinsic and extrinsic stacking faults in face-centered cubic structure [24]. This argument has been confirmed in Ti_4AlN_3 [23].

MAX phases are well-known for their anisotropic chemical bonding. The M—X is significantly stronger than M—A [2], enabling them to be mechanically and chemically exfoliated to produce MXene [25,26]. For the nanolaminated MAX phases, shear along non-basal plane means breaking the edge-sharing M_6X octahedrons and hence this kind of deformation is extremely energetically unfavorable. Theoretical calculations have demonstrated that the energy for shearing Ti—N is 2~3 times higher than that for shearing Ti—Al along $\langle 11\bar{2}0\rangle$ [21]. The height of cleavage terraces in V_2AlC and Cr_2AlC has been measured to be an integer number of half-lattice units [27,28], suggesting that the cleavage of basal plane occurs possibly between the MX layers and the dislocation core is therefore proposed to be there. However, a direct experimental evidence is hitherto still unavailable. In this letter, we address this issue by studying the nature of dislocations and stacking faults in $Nb_{12}Al_3C_8$, a carbon-vacancy-ordered MAX phase.

The sample was synthesized by the method reported in Ref. [29]. The as-prepared sample was annealed at 1200 °C for 50 h to ensure the carbon-vacancy fully ordered. Room-temperature neutron diffraction analysis was carried out on a neutron powder diffractometer using a wavelength of $\lambda = 1.57$ Å with a step of 0.075° at the Institute of Nuclear Physics and Chemistry, China. Cylinders with a dimension of Φ6.5 mm × 8.5 mm machined from the as-annealed sample were heated up to 1400 °C at a heating rate of 5 °C/s in vacuum, then held

* Corresponding authors.
E-mail addresses: wang@imr.ac.cn (X. Wang), yzchou714@gmail.com (Y. Zhou).

https://doi.org/10.1016/j.scriptamat.2017.10.020
1359-6462/

5 min and compressed 15% at a strain rate of 10^{-4}/s using Gleeble 3800 (DSI, Poestenkill, NY). The microstructures were examined by a scanning electron microscope (LEO, SUPRA55, Ammerbuch, Germany) with electron backscatter diffraction (EBSD) technique. Dislocation configurations were investigated by a transmission electron microscope (FEI, Tecnai G2 F20, Oregon, USA). A Titan^{3}™ G^{2} 60–300 aberration-correction TEM operated at 300 kV was used to collect high-resolution high-angle annular dark-filed (HAADF) scanning transmission electron microscopy (STEM) images. Geometric phase analysis (GPA) [30] was applied to reveal strain field.

Fig. 1(a) shows the typical scanning electron microscopy (SEM) image of the as-prepared sample. The bar-like grains are ~50 μm in length and ~10 μm in width. The grain boundaries are predominantly large angle boundaries [31]. Interestingly, the misorientation-angle distribution in Fig. 1(b) demonstrates a striking peak around 30°. The misorientation-axis distribution for 28° ~ 32° in the inset suggests a [0001] rotation axis. At first glance, this type of boundary is unusual because the well-documented tilt boundaries in MAX phases are kinking boundaries with ⟨11$\bar{2}$0⟩ as the rotation axis [11]. In the as-prepared Nb_4AlC_{3-x}, there are numerous order-disorder domains due to the co-existence of carbon-vacancy-ordered phase ($Nb_{12}Al_3C_8$) and carbon-vacancy-disordered phase (α-Nb_4AlC_{3-x}), wherein the crystallographic orientation relationship is [1$\bar{2}$10] $Nb_{12}Al_3C_8$ ∥ [1$\bar{1}$00] α-Nb_4AlC_{3-x}, [0$\bar{1}$10] $Nb_{12}Al_3C_8$ ∥ [1$\bar{2}$10] α-Nb_4AlC_{3-x}. The majority of diffractions are overlapped and thus the EBSD cannot differentiate the two phases, and the EBSD software interprets the domain boundary as 30°/[0001] grain boundary. In Fig. 1(c), the 30°/[0001] domain boundaries are highlighted in black segments. Among the grains in the field of view, the domain boundaries are non-homogeneous. For example, the density of domain boundaries in the filled arrow marked grain is very high while the hollow arrow marked grain has nearly no domain boundaries. The TEM morphologies in Fig. 1(d) imaged with (10$\bar{1}$0) diffraction of $Nb_{12}Al_3C_8$ reveal that the domains, dark grey regions, exhibit irregular shapes. In the as-prepared sample, $Nb_{12}Al_3C_8$ and α-Nb_4AlC_{3-x} account for ~81 vol% and 19 vol%, respectively. After annealing at 1200 °C for 50 h, the absence of dark grey contrasts as shown in Fig. 1(e) implies that all α-Nb_4AlC_{3-x} transforms to $Nb_{12}Al_3C_8$. Accordingly, the 30°/[0001] boundaries were barely observed in the EBSD characterizations (not shown here for conciseness). Fig. 1(f) provides the neutron diffraction pattern of the as-annealed sample, where the ordering peaks (10$\bar{1}$0) and (10$\bar{1}$2) of $Nb_{12}Al_3C_8$ are clearly identified as shown in the inset. The annealed sample was used for deformation and dislocation analysis.

Dislocations in the deformed $Nb_{12}Al_3C_8$ are quite inhomogeneous. For some grains, the dislocation density can be an order of 10^{9}/cm^{2}, while for the others dislocations are nearly absent. For the sake of simplicity, dislocation networks shown in Fig. 2(a) are chosen for

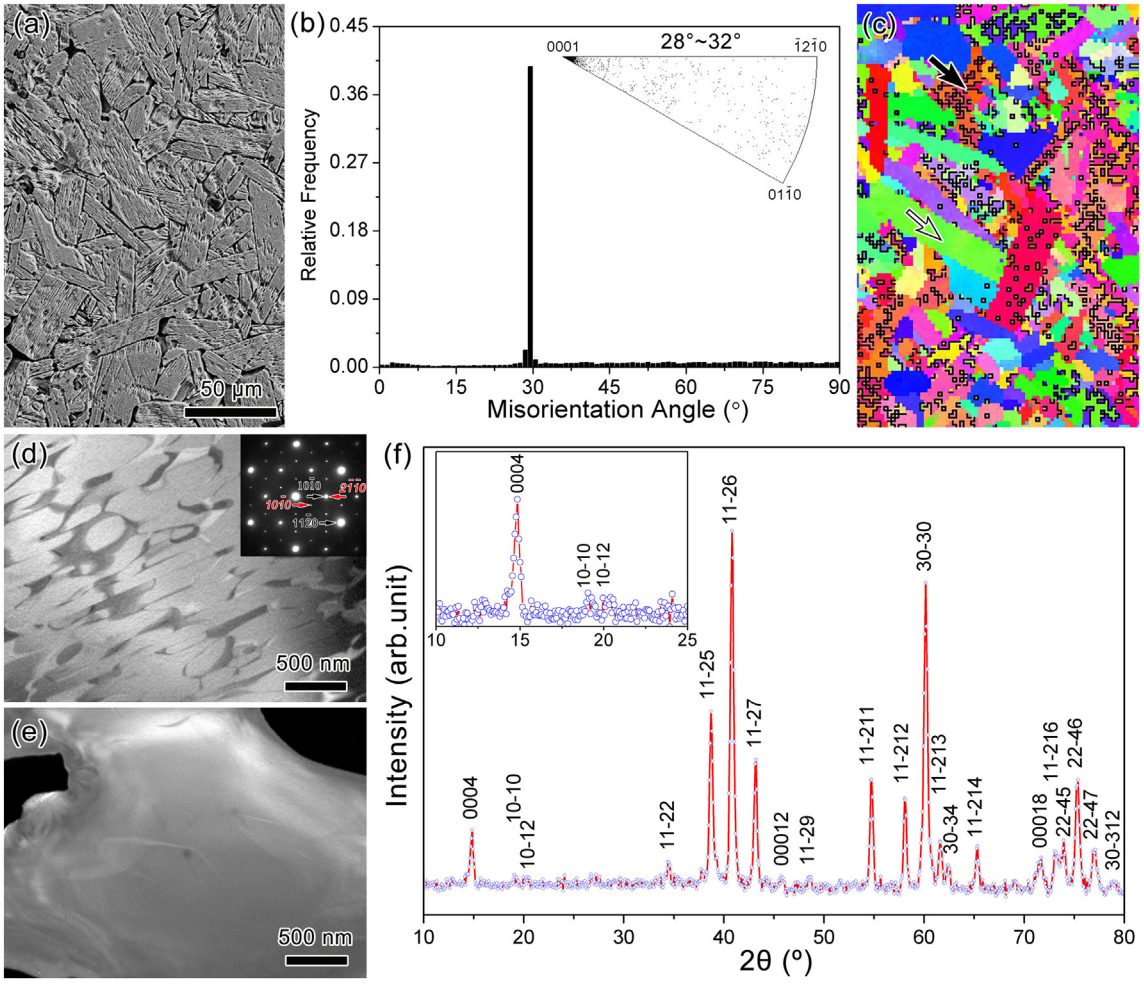

Fig. 1. (a) SEM morphology of etched surface. (b) Distribution of misorientation angle and axis (inset) of the as-prepared sample. (c) EBSD map with inverse pole figure color-coding. The 30°/[0001] boundaries are highlighted with black lines. (d,e) Typical TEM dark-field morphologies of the (d) as-prepared and (e) annealed sample. Inset in (d) is the selected area electron diffraction pattern. The black and red indexes are indexed with $Nb_{12}Al_3C_8$ and α-Nb_4AlC_{3-x}. Superlattice diffraction spot (10$\bar{1}$0) of $Nb_{12}Al_3C_8$ was used for dark-field imaging. (f) Neutron diffraction pattern of the annealed sample. Inset shows the superlattice diffraction peaks (10$\bar{1}$0) and (10$\bar{1}$2). (For interpretation of the references to color in this figure legend, the reader is referred to the web version of this article.)